# Disambiguation of Uniform Demagnetization Fault from Position Sensor Fault in FOC PMSM Applications

Sandun S. Kuruppu, *Senior Member, IEEE* and Sunil G. Abeyratne*, Senior Member IEEE*

*Abstract*—Electrification of higher torque density applications in the transportation sector and robotics sector are primarily met with permanent magnet synchronous machines (PMSMs), attributing to their unique properties. However, wide operating temperatures, field weakening controls, and low-quality magnets, lead to uniform demagnetization of rotor magnets. Demagnetization in torque control applications reduce the effective output torque as the output torque is proportional to rotor flux level. Detection of such rotor demagnetization is essential and only second to few key faults from the system perspective. A simple and common approach to detect uniform demagnetization in a sensored-FOC PMSM drive system in torque control mode is discussed in this paper with experimental results emulating uniform demagnetization effect. The false positive nature in the proposed algorithm under a position sensor offset error is discussed, followed by a disambiguation strategy, which are primary contributions of this paper. Analysis, simulation and experimental results are presented to validate the proposed disambiguation strategy.

*Index Terms*—permanent magnet synchronous motors, demagnetization diagnosis, fault disambiguation, fault detection, machine vector control, position measurement

## NOMENCLATURE

| | |
|---|---|
| $\lambda_m'^r$ | Flux linkage coefficient |
| $\theta_r$ | Motor rotor position |
| $E_{as}(\theta_r)$ | Phase A back electromotive force (EMF) |
| $E$ | Magnitude of fundamental back EMF component |
| $\varphi_k$ | Phase of the $k^{th}$ back EMF harmonic |
| $k$ | Harmonic order |
| $e_k$ | Magnitude of the kth back EMF component |
| $\widehat{\lambda_m'^r}$ | Uniformly demagnetized flux linkage coefficient |
| $\Delta\lambda_m'^r$ | Change in flux linkage coefficient |
| $V_{qs}^r, V_{ds}^r$ | Quadrature and direct axis voltages |
| $I_{qs}^r, I_{ds}^r$ | Quadrature and direct axis currents |
| $I_{as}, I_{bs}$ | Phase A and Phase B currents |
| $r_s$ | Phase resistance |
| $L_q, L_d$ | Quadrature and direct axis inductance |
| $\omega_r$ | Rotor speed |
| $K_P$ | Proportional gain of PI controller |
| $K_I$ | Integral gain of PI controller |
| $P(s)$ | PMSM model under synchronous frame |
| $C(s)$ | Proportional and integral (PI) controller |
| $\Delta\theta$ | Position sensor offset error |
| $i_{qs}^r$ | Quadrature axis current |
| $i_{ds}^r$ | Direct axis current |
| $V_{qs\_m}^r$ | Quadrature axis voltage applied to the motor |
| $V_{ds\_m}^r$ | Direct axis voltage applied to the motor |
| $V_{qs\_Err}^r$ | Quadrature axis voltage error |
| $V_{ds\_Err}^r$ | Direct axis voltage error |

## I. INTRODUCTION

ELECTRIFICATION in the transportation sector has outgrown the powertrain and into many other subsystems. Historically transition to an electromechanical energy conversion system was driven by efficiency. However, more recently the ease of interfacing with artificial intelligence (AI) has become another advantage. With the success of electrification in the ground transportation sector, the next leap is to address efficiency and reliability challenges in the aerospace industry through electrification. Ground as well as aerospace transportation application subsystems such as propulsion/powertrain, steering, power generation, thermal management and air conditioning systems are being converted to electric. Numerous other industries such as robotics, manufacturing and consumer products are also rapidly growing in size, fueled by the mechatronic systems integrated with AI. Among the machines popular for electromechanical energy conversion, permanent magnet synchronous machines (PMSMs) have proven to be advantageous. Despite the cost of rare earth magnets, higher torque density, compact design, better thermal characteristics, and simple, high dynamic control are factors in favor of PMSMs.

Electric machines used in powertrain, aerospace propulsion, power generation units, and steering systems are subjected to high temperature conditions, high currents and field weakening control to achieve higher speeds without increasing the DC link

S.S. Kuruppu is with the Saginaw Valley State University, University Center, 48710 USA (e-mail: skuruppu@svsu.edu).

S.G. Abeyratne is with University of Peradeniya, Sri Lanka (e-mail: sunil@ee.pdn.ac.lk).

voltage. However, subjecting a PMSM to such conditions demagnetizes the rotor magnets to a certain degree over prolonged use [1]-[3]. Further, manufacturing defects may also contribute to accelerating the demagnetization process [4]. With all magnets on the rotor being subjected to field weakening, the demagnetization effect can be represented by a significant reduction in the fundamental flux linkage and added harmonic content on flux linkage constant ($\lambda_m^{\prime r}$ is the flux linkage constant amplitude). Demagnetization is easily observed through back EMF profile of a machine as the back EMF is a function of speed and flux linkage (1). The harmonic content is caused by the slight variations of magnet properties between the magnets on the rotor. Figure 1 illustrates an example of how demagnetization maybe represented by back EMF at a constant speed.

$$E_{as}(\theta_r) = E\sin(\theta_r + \varphi_1) + e_0 + \sum_{k=2}^{\infty} e_k \sin(k\theta_r + \varphi_k) \quad (1)$$
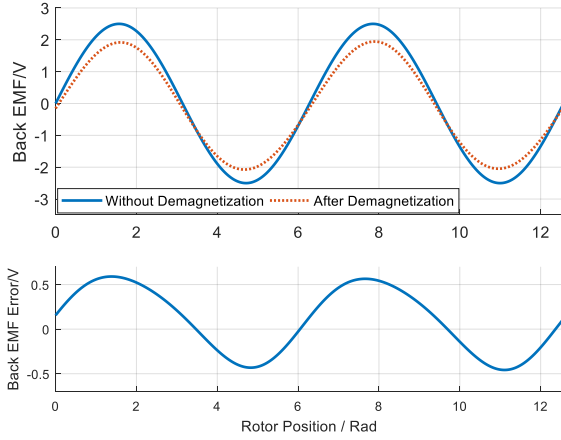


Fig. 1. Back EMF profile example under demagnetization at constant speed

In this scenario a uniform demagnetization effect is considered as all magnets on the rotor are subjected to the opposing flux generated by the stator used for field weakening. Therefore, it is assumed that the flux linkage coefficient is reduced introducing a reduction in the back EMF amplitude as in (2). The DC offset and the higher order harmonics are assumed to be negligible. $\widehat{\lambda_m^{\prime r}}$ is the flux linkage constant amplitude after demagnetization.

$$\widehat{\lambda_m^{\prime r}}\sin(\theta_r) \approx \lambda_m^{\prime r}\sin(\theta_r) - \Delta\lambda_m^{\prime r}\sin(\theta_r) \quad (2)$$

Reduced flux linkage constant implies that the machines torque constant has also reduced, resulting in lower torque output at the same regulated current in torque-controlled applications. In speed-controlled applications, higher current will be injected to obtain the same levels of torque, increasing the losses in the system and consequently the operating temperature, accelerating demagnetization. Therefore, detecting significant amount of uniform demagnetization is essential to sustain system performance and efficiency. Uniform demagnetization detection in applications are achieved through several different strategies [1]-[5]. Among them, the quadrature axis voltage measurement is a common approach in industry. However, this method results in a false

positive under static position sensor offset error (PSOE), which is a severe fault by itself. Due to symmetric nature of uniform demagnetization and PSOE, a proper disambiguation strategy needs to be devised. This paper presents a strategy to easily disambiguate between uniform disambiguation and PSOE through model-based signature analysis.

The paper is organized as follows. Section II summarizes existing body of work on demagnetization detection and their inability to distinguish PSOE, section III discusses the demagnetization problem mathematically, while emphasizing common uniform demagnetization detection strategy. Section IV provides both experimental and simulation results on how the demagnetization fault behave followed by section V detailing demagnetization detection algorithm. Section VI discusses how PSOE causes false positives in demagnetization detection algorithm and proposes a disambiguation strategy. Section VII concludes the paper with final remarks.

## II. EXISTING RESEARCH

Demagnetization detection in PMSMs have been studied by number of researchers and discussed here to emphasize the significance of the research presented in this paper. Zhao et al in [6] propose an adaptive linear neuron model reference adaptive system for uniform demagnetization detection in a linear PMSM through flux linkage observation. A Series of demagnetizations are considered for model evaluation under different speed, in a speed-controlled application. Three different algorithms are also compared for their accuracy. However, the complexity of these proposed algorithms renders them impractical for many applications. The authors of [5] propose a real time demagnetization assessment method for PMSMs based on a transfer inductance matrix. The demagnetization assessment is made based on a first order approximation of the demagnetization characteristics under varying parameter levels such as current references, resulting in a temperature estimate. An α-β subspace harmonic mapping based uniform demagnetization detection in PMSM is proposed in [7]. The authors propose 5th harmonic component as a means to detect uniform rotor magnet demagnetization in six phase surface mount PMSMs. A search coil-based winding failure and demagnetization detection is proposed in [8]. However, the results are only based on finite element analysis. Hong et al in [9] propose a strategy to detect PMSM rotor faults using a test embedded in the inverter to be used when the machine is not in operation. The approach is using a signal injected through the d-axis current to classify and identify faults. Typically, such off-state testing is not conducted in consumer applications such as automotive due to safety concerns and prevents the detection of a fault that occurred during normal operation (during run time). Frequency domain approaches such as wavelet-based fault detection has been widely proposed for demagnetization diagnosis in [10]-[13]. Asymmetric magnet fault detection using leakage flux is proposed in [14]. A fluxgate sensor, which is a special type of sensor is used to measure leakage which are otherwise difficult to measure. Harmonic content visible on the leakage flux spectra are used to detect these asymmetric magnet failure modes such as broken magnets. Zhu et al proposes a flux

based acoustic noise model for demagnetization and a back propagation neural network to detect demagnetization based on acoustic data. The authors claim that the method is computationally efficient and not sensitive to machine parameters [15][16]. However, it is not clear how authors justify the claims as machine parameters vary in a mass-manufacturing environment causing the harmonic amplitudes to change. Further, frequency domain spectrum generation requires high computational power, which may not be available on consumer applications. [1] presents a summary of available techniques and emphasizes the difficulty in detecting uniform demagnetization through motor current signature analysis. Further, frequency domain harmonics maybe caused by other types of faults too. Considering the significance and nature of a demagnetization fault, a simple rotor reference frame voltage-based approach is feasible. Further, previous work fails to identify how a static position offset error may result in a false positive demagnetization fault if not properly distinguished. Hence this paper proposes a uniform demagnetization strategy using real-time signals along with a disambiguation strategy from position sensor offset error fault. The proposed approach is for a sensored field-oriented controlled (FOC) PMSM used in a torque control application.

## III. DISCUSSION ON SIMPLE UNIFORM DEMAGNETIZATION DIAGNOSIS AND QUANTIFICATION STRATEGY

A field oriented controlled PMSM system block diagram in a torque-controlled application is shown in figure 2. The dynamic model equations of a PMSM in rotor reference frame are given in (3) and (4). A position sensor is used to measure rotor position and orient stator flux for optimal torque generation. Proportional and integral regulators (PI regulators) are used to maintain the required currents based on torque demand.
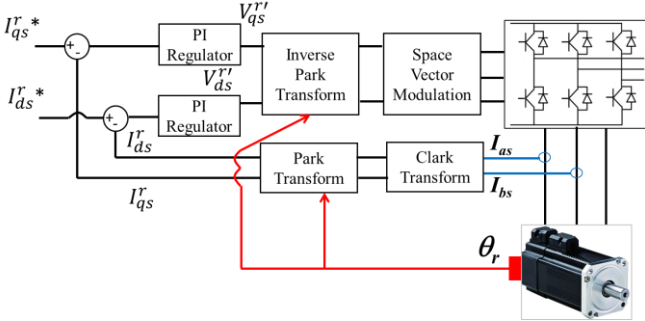


Fig. 2. Field oriented control algorithm with position sensor

$$V_{qs}^r = L_q \frac{di_{qs}^r}{dt} + r_s i_{qs}^r + \omega_r L_d i_{ds}^r + \omega_r \lambda_m'^r \tag{3}$$

$$V_{ds}^r = L_d \frac{di_{ds}^r}{dt} + r_s i_{ds}^r - \omega_r L_q i_{qs}^r \tag{4}$$

For the purpose of analysis, the FOC system maybe viewed as a two state, state-space representation in matrix form. Assuming the position sensor offset is accurately calibrated, and the inverter is a linear plant of unity gain, the system block diagram for the proposed representation is as follows.
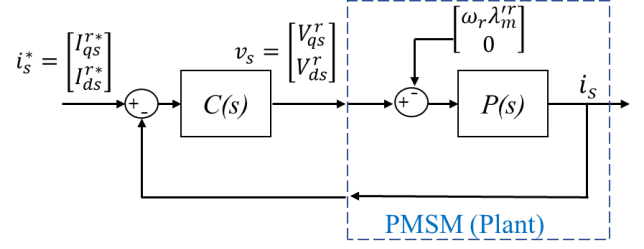


Fig. 3. Simplified block diagram of Field oriented control algorithm with position sensor for analysis

C(s) and P(s) are as follows,

$$C(s) = \begin{bmatrix} (K_P s + K_I)/s & 0 \\ 0 & (K_P s + K_I)/s \end{bmatrix} \tag{5}$$

$$P(s) = \begin{bmatrix} r_s + sL_q & \omega_r L_d \\ -\omega_r L_q & r_s + sL_d \end{bmatrix}^{-1} \tag{6}$$

In order to identify the effect of the demagnetization, voltage applied to the motor ($v_s$) is considered. The following closed loop transfer function may be obtained for the above system shown in figure 3.

$$\begin{bmatrix} V_{qs}^r \\ V_{ds}^r \end{bmatrix} = \frac{C(s)}{[I + C(s)P(s)]} \begin{bmatrix} I_{qs}^{r*} \\ I_{ds}^{r*} \end{bmatrix} + \frac{C(s)P(s)}{[I + C(s)P(s)]} \begin{bmatrix} \omega_r \lambda_m'^r \\ 0 \end{bmatrix} \tag{7}$$

Considering the step input response of a healthy system (i.e., no uniform demagnetization) at steady state, the above relation reduces to (8).

$$\begin{bmatrix} V_{qs}^r \\ V_{ds}^r \end{bmatrix} = \begin{bmatrix} r_s & \omega_r L_d \\ -\omega_r L_q & r_s \end{bmatrix} \begin{bmatrix} I_{qs}^{r*} \\ I_{ds}^{r*} \end{bmatrix} + \begin{bmatrix} 1 & 0 \\ 0 & 1 \end{bmatrix} \begin{bmatrix} \omega_r \lambda_m'^r \\ 0 \end{bmatrix} \tag{8}$$

However, in the situation where uniform demagnetization has occurred, the rotor reference frame voltages applied to the motor are given by (9). Note that true motor currents are used in (9) assuming PI regulators are properly regulating the requested current references. It is evident that with uniform demagnetization, the applied q-axis voltage reduces. $V_{qs\_m}^r$ and $V_{ds\_m}^r$ represent the rotor reference frame voltage generated by the PI regulators that are applied to the motor via the inverter. These values are available in the controller itself and no additional measurement is needed.

$$\begin{bmatrix} V_{qs\_m}^r \\ V_{ds\_m}^r \end{bmatrix} = \begin{bmatrix} r_s & \omega_r L_d \\ -\omega_r L_q & r_s \end{bmatrix} \begin{bmatrix} I_{qs}^r \\ I_{ds}^r \end{bmatrix} + \begin{bmatrix} 1 & 0 \\ 0 & 1 \end{bmatrix} \begin{bmatrix} \omega_r \widehat{\lambda_m'^r} \\ 0 \end{bmatrix} \tag{9}$$

Rotor reference frame voltages shown in (8) can be calculated given the motor parameters, motor speed and reference currents. The difference between the voltages applied to the motor and the voltages computed based on the model will emphasize the voltage difference induced by the demagnetization as in (10).

$$\begin{bmatrix} V_{qs\_err}^r \\ V_{ds\_err}^r \end{bmatrix} = \begin{bmatrix} V_{qs}^r - V_{qs\_m}^r \\ V_{ds}^r - V_{ds\_m}^r \end{bmatrix} = \begin{bmatrix} \omega_r(\lambda_m'^r - \widehat{\lambda_m'^r}) \\ 0 \end{bmatrix} \tag{10}$$

4

$$V_{qs\_err}^r / \omega_r = \lambda_m'^r - \widehat{\lambda_m'^r} \qquad (11)$$

Speed normalized quadrature axis voltage error as shown in (11), indicates the error in flux linkage constant. In practical applications, machines tend to operate outside magnetically linear region causing the flux linkage constant to change, causing a false positive demagnetization fault. A sufficiently accurate flux linkage coefficient profile as a function of machine current during calibration phase will eliminate such false positives. The following section provides simulation and experimental results for the uniform demagnetization diagnosis approach.

## IV. SIMULATION AND EXPERIMENTAL RESULTS OF DEMAGNETIZATION FAULT BEHAVIOR

### A. Simulation Results

Prior to experimental validation, Matlab Simulink based simulations were conducted to validate the proposed strategy. The system used for the simulation study closely models the experimental setup to be discussed in part b, below. The PMSM is operated in torque control mode, while the mechanical system speed is maintained constant by a dynamometer.

Figure 4 illustrates the effect of varying uniform demagnetization on rotor reference frame voltage errors discussed in (10). Simulations results in figure 4 are at varying uniform demagnetization levels, while the speed is held constant. Simulation data was collected under six different speed settings. First subplot depicts the quadrature axis current which is regulated at 1A. Second subplot is representing the variation of flux linkage coefficient, at each level of demagnetization. Third and fourth subplots indicate the behavior of the rotor reference frame voltage errors at each operating condition (as in (10)).
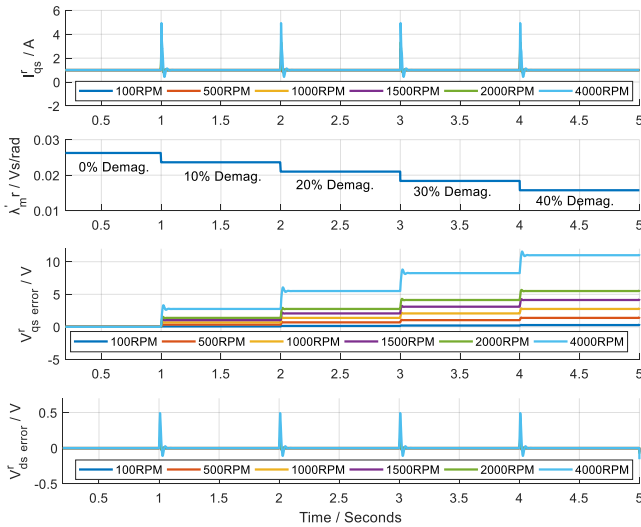
Fig. 4.  Uniform demagnetization detection error with varying speed

The transients visible in the current and voltage plots are caused by the closed loop system response to the introduced demagnetization and regulating current at the intended reference value. Simulation results in figure 4 justify the relation obtained in analysis, demonstrating the proportional

increase of quadrature axis voltage error, along with increasing demagnetization.
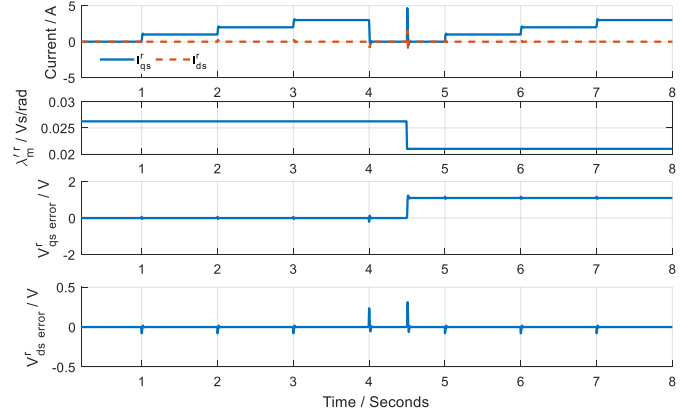
Fig. 5.  Uniform demagnetization detection error with varying current

Figure 5 illustrates the response of rotor reference frame voltage errors with varying quadrature axis current reference while the speed and the demagnetization level are maintained constant. As seen in the first subplot of figure 5, the quadrature axis current is increased in steps of 1A. Direct axis current is regulated to be at 0A. The second subplot shows the variation in flux linkage coefficient (i.e. demagnetization level). A 20% demagnetization is introduced at *t=4.5 seconds*. Motor speed is maintained constant at 2000RPM during this test. According to simulations, there is no influence of motor current on the proposed demagnetization detection scheme.

### B. Experimental Results

Experimental validation of the proposed method is presented here. The experimental setup is depicted in figure 6 followed by the parameters of the PMSM in Table I. The PMSM is coupled to a DC machine through an in-line torque sensor. Both machines are controlled with dSPACE DS1104 R&D platform shown. The PMSM is operated in field oriented controlled torque mode, where as the DC machine is speed regulated. The demagnetization detection as well as the demagnetization effect emulation was also implemented on the same dSPACE platform. dSPACE systems is a rapid prototyping platform facilitated by Matlab Simulink based auto coding. The underlying DSP is a MPC8240 processor with PPC 603e core operating at 250MHz clock.
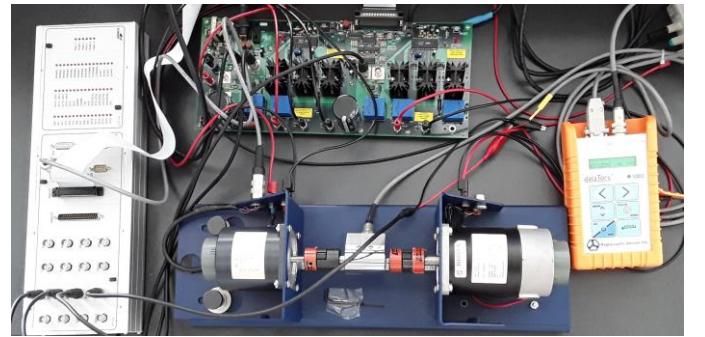
Fig. 6.  PMSM demagnetization algorithm validation setup with torque sensor

TABLE I
PMSM PARAMETERS

| Parameter | Value |
|---|---|
| Poles | 10 |
| Rated voltage | 42V |
| Phase Resistance ($r_s$) | 0.2239 Ω |
| Q-axis Inductance ($L_q$) | 367.2 µH |
| Back EMF Constant ($\lambda_m'^r$) | 0.0122 V/(rads$^{-1}$) |

According to (11), under uniform demagnetization, $\widehat{\lambda_m'^r} < \lambda_m'^r$. Therefore, $V_{qs\_m}^r < V_{qs}^r$. $V_{qs}^r$ is a computed value based on motor parameters, current references and motor speed, according to (8) to be compared with the applied voltage in rotor reference frame, which is $V_{qs\_m}^r$. However, demagnetizing a machine is permanent and makes the machine useless for future research. Hence, for the purpose of algorithm validation, uniform demagnetization was emulated by achieving $V_{qs\_m}^r < V_{qs}^r$ condition through modifying the $\lambda_m'^r$ value to be larger than the nominal value. For dynamometer testing, this was deemed acceptable as the faulty motor is acting as the torque regulator and the dynamometer (DC motor) is regulating speed, which matches the torque on the faulty PMSM.

Figure 7 through 9 depict experimental results on how the emulated uniform demagnetization effect is reflected on the quadrature and direct axis voltage error. Since uniform demagnetization of a PMSM is permanent, and renders the machine unusable, characteristics similar to demagnetization was emulated based on the result in (10). Under a uniform demagnetization effect, the flux linkage coefficient changes from $\lambda_m'^r$ to $\widehat{\lambda_m'^r}$. Therefore, to evaluate the proposed algorithm and the disambiguation strategy, the flux linkage coefficient used by the rotor reference frame (RRF) voltage error calculation was varied. In doing so, the proposed algorithm experiences an effect similar to a uniform demagnetization, allowing for algorithm development without permanently demagnetizing the PMSM.

Figure 7 depicts the variation of RRF voltages under different emulated demagnetization conditions and varying speeds. For each test, the speed was maintained constant while the demagnetization level is increased from 0% to 40% in increments of 10%. PMSM current reference was maintained constant with $I_{qs}^{r*} = 1A$ and $I_{ds}^{r*} = 0$ (subplot 1). Second subplot represents the level of demagnetization. Third and fourth subplots are for $V_{qs\_err}^r$, $V_{ds\_err}^r$, respectively. The q-axis voltage errors follow (11), showing that increasing speed results in higher voltage error for uniform demagnetization detection. No significant variation is observed on the direct axis voltage error.
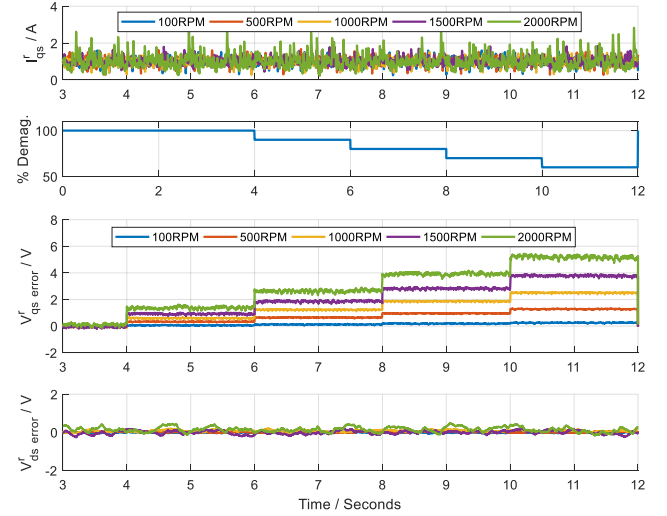


Fig. 7. Rotor reference frame voltage error variation at different emulated demagnetization levels with varying speed

The effect of varying current reference under two different demagnetization scenarios are studied in figure 8. The speed of the PMSM was maintained at 500RPM, while the current reference was changed from 0A to 3.5A in steps of 0.5A. First subplot of figure 8 show the regulated motor current. Second and third subfigures, depict the variation of RRF voltage errors. Unlike simulations, the quadrature axis voltage error (Figure 8 second subplot) shows a slight variation due to the varying current references. The is primarily due to the level of air gap flux changing with changing current reference and non-linear saturation characteristics. The simulation assumes an ideal machine and therefore does not demonstrate a similar effect. A simple look up table-based voltage error compensation strategy was implemented to correct for the error introduced by magnetic non-linearities at varying current levels. The look-up table implementation is shown in figure 10.
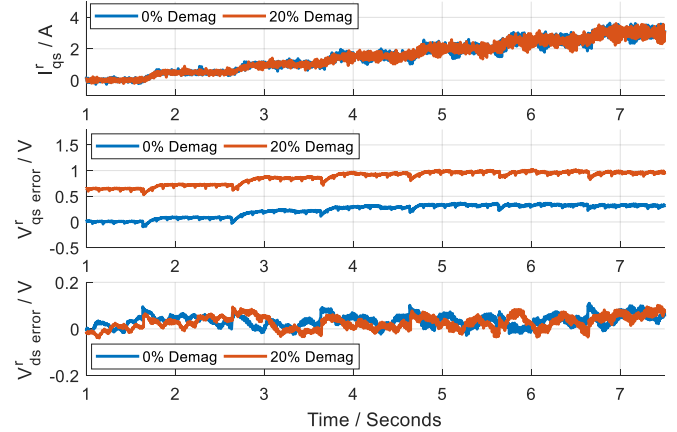


Fig. 8. Rotor reference frame voltage error variation at different emulated demagnetization levels with varying current references at 500RPM. (without non-linearity compensation)
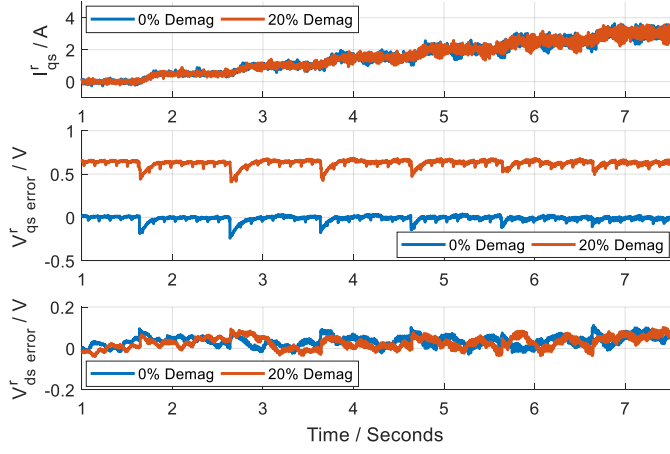
Fig. 9. Rotor reference frame voltage error variation at different emulated demagnetization levels with varying current references at 500 RPM (with current reference based non-linearity compensation)

The reference current used by the FOC algorithm was used as the input to the look up table to prevent additional noise from influencing the demagnetization detection algorithm. Results after the current based compensation are shown in figure 9. It is evident that the results with current based compensation show no variation of voltage error with varying current.

The updated uniform demagnetization detection algorithm is provided in the block diagram below (Figure 10). The block diagram also includes transient blocking and a threshold setting to trigger a uniform demagnetization fault flag. Simulation results and experimental results under varying conditions are illustrated in figures 11 through 13.
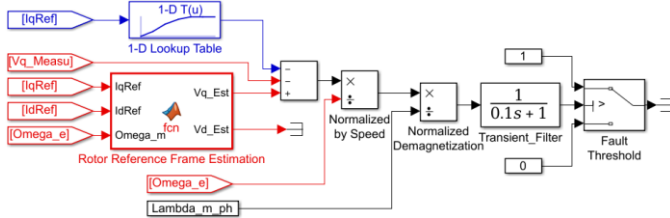


Fig. 10. Implementation of the proposed demagnetization detection method

## V. SIMULATION AND EXPERIMENTAL RESULTS OF DEMAGNETIZATION DETECTION

Characteristics of the demagnetization detection algorithm is presented under different scenarios to demonstrate the behavior under transient states. Figure 11 illustrates simulation results at different operating points, with uniform demagnetization fault being injected between $t = 2\ seconds$ to $t = 4\ seconds$. From $t = 0\ seconds$ to $t = 2\ seconds$, the current reference is being changed to illustrate that there is no false positive caused by current transients in the demagnetization detection algorithm. The results shown after $t > 4.5\ seconds$ illustrate how position sensor offset error (PSOE) influences the fault diagnosis system and this will be discussed in the next section, as it relates to the false positive causes and disambiguation. Fourth subplot in figure 11 depicts the normalized uniform demagnetization signal with 5th and 6th subplots being fault detection flags for uniform demagnetization and disambiguation, respectively.
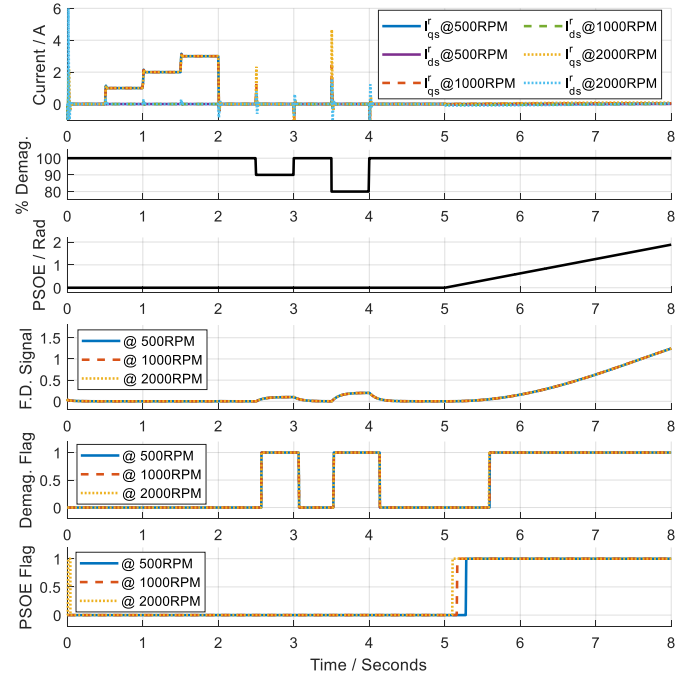


Fig. 11. Simulation results of the proposed demagnetization detection method at varying currents and speeds

Figure 12 is an experimental validation of the demagnetization detection scheme discussed above. A 20% uniform demagnetization is introduced at 500RPM and 1A of quadrature axis current. The fault diagnosis signal (F.D. Signal in fourth subplot) is experiencing an increase, followed by the Fault flag being set (fifth subplot). The flag and the F.D. signal subside, immediately after the demagnetization fault is removed.

Figure 13 experimentally evaluates to see if current transients cause any false positives in the proposed fault diagnosis approach. At 500RPM, the current reference is being changed from 1A to 2A and then to 3A. Despite the transients in the F.D. signal, the threshold and filtering used in the proposed algorithm help mitigate potential false positives caused by current transients.
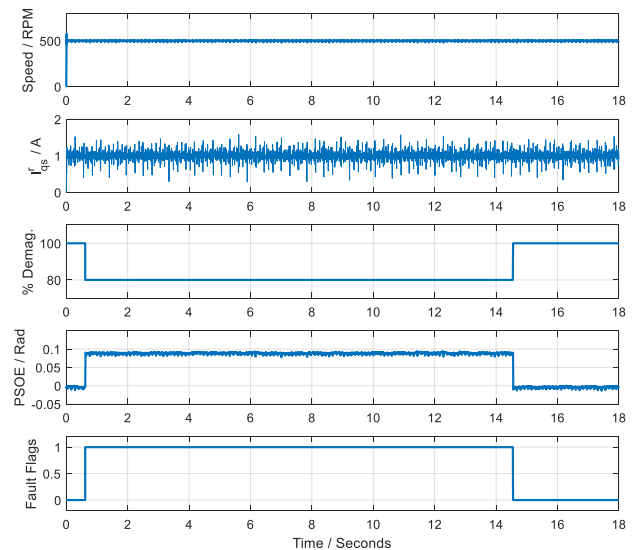


Fig. 12. Experimental implementation results of the rotor reference frame based demagnetization detection method
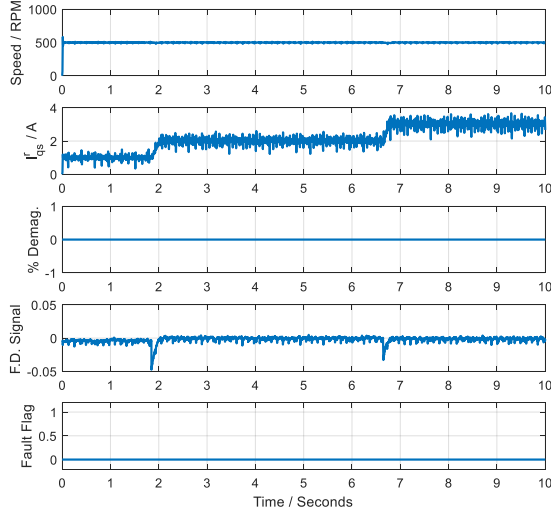
Fig. 13. Current transient handling of the demagnetization detection method

Both simulation and experimental result shown above validate the capability of the demagnetization detection strategy to identify uniform demagnetization. However, there is a potential source of false positive that need to be addressed. This is discussed in the next section.

## VI. EFFECT OF PSOE ON DEMAGNETIZATION DETECTION AND DISAMBIGUATION STRATEGIES

FOC controlled PMSMs require rotor position information for optimal stator field orientation and commutation. However, as discussed in [17]-[19], position sensor measurement may contain a DC offset (PSOE: position sensor offset error) and/or harmonic content. Of these, the PSOE has a significant impact on system torque output, along with the potential to cause a false positive in demagnetization detection approach(s). Experimental result below supports the above argument. Figure 14 illustrates the behavior of $V_{qs\_err}^r$ and $V_{ds\_err}^r$ discussed in (10) during a varying PSOE at different speeds. The varying PSOE value is shown in the first subplot of figure 14. The effect is only amplified at higher speed as seen by the increasing voltage error amplitudes in subplot 3 and 4.
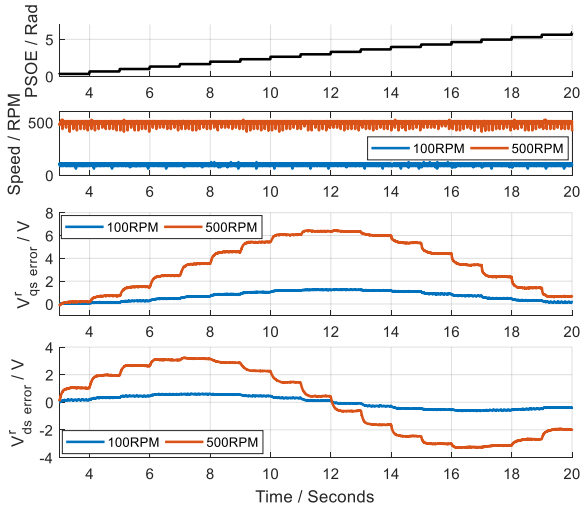


Fig. 14. Effect of PSOE on signals used for demagnetization detection

The effect of PSOE on the uniform demagnetization detection method is shown in figures 11 (simulation) and 15 (experimental). Motor speed is maintained at 500RPM and the current is regulated at 1A. The demagnetization percentage is held at 0% while a PSOE is being injected to the system artificially. The PSOE, as shown in fourth subplot, is being varied from zero to $2\pi$ radians in steps of 0.331 radians. The fifth subplot is the uniform demagnetization fault diagnosis signal ($V_{qs\_err}^r$), followed by the uniform demagnetization detection flag in the 6th subplot. Since demagnetization fault and PSOE cause the $V_{qs\_err}^r$ to rise, a disambiguation strategy is needed to identify the two faults independently. The primary difference between the two faults is that the PSOE gives rise to $V_{ds\_err}^r$ whereas a uniform demagnetization has no effect on this signal. Therefore, a second fault flag is generated based on $V_{ds\_err}^r$ signal deviation from a threshold voltage, to disambiguate between the two faults.
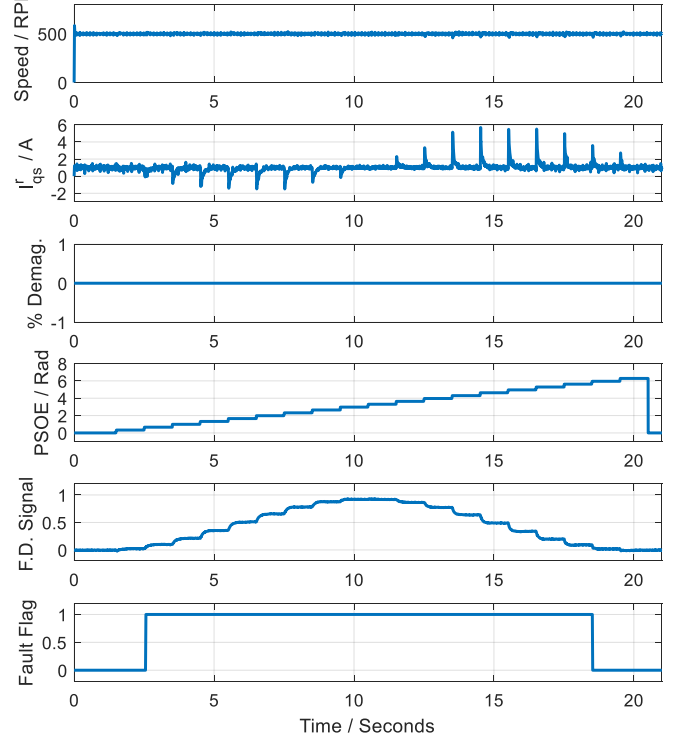


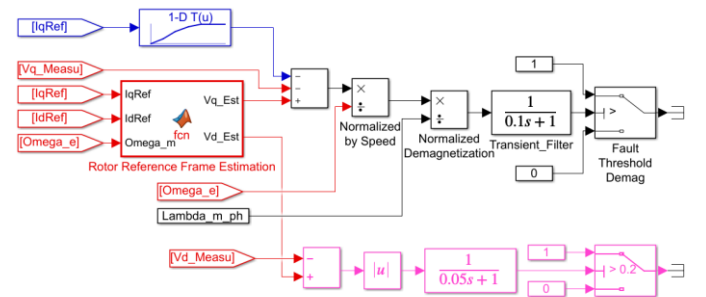Fig. 15. Experimental results on false positive uniform demagnetization caused by PSOE



Fig. 16. Improved demagnetization detection with PSOE disambiguation

The disambiguation flag implementation is shown in the proposed addition in figure 16. The direct axis voltage error is

filtered and compared with a set threshold for the second flag. Therefore, when a PSOE is introduced to the system, both demagnetization detection flag and PSOE fault flag will be set. Figure 11 (*t > 5 seconds*), shows simulation results on the disambiguation strategy. Results shown in figure 17, experimentally demonstrate the function of the proposed demagnetization detection and disambiguation. Subplot 4 indicates the injection of PSOE with fifth subplot indicating the behavior of the two flags enabling the disambiguation of a uniform demagnetization fault from a PSOE fault. Filters and threshold selection are used to block potential false positives caused by transients. Therefore, the fault detection may not be possible for a minute range of the fault diagnosis signal, which is unavoidable and a limitation in the proposed disambiguation strategy.
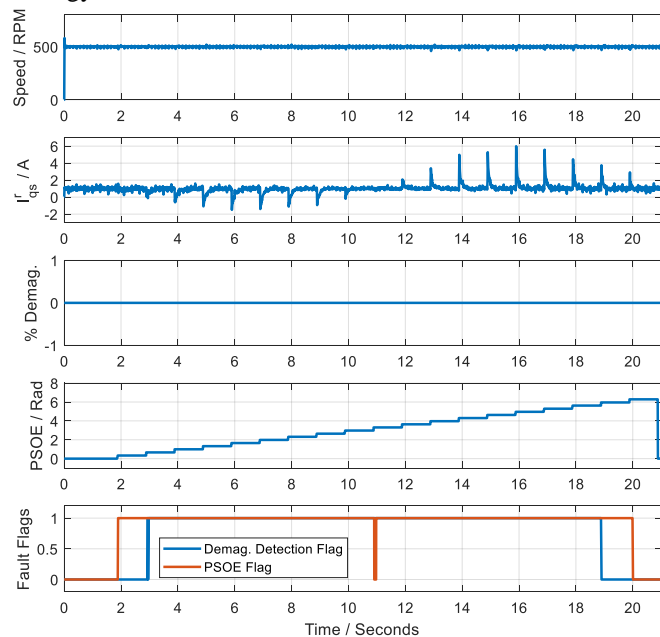


Fig. 17. Experimental results on the improved demagnetization detection with PSOE disambiguation

## VII. CONCLUSION

PMSMs are widely used in applications requiring high torque density and high dynamic controls. However, the magnets used in PMSM rotors, may experience uniform demagnetization under high operating temperature, extensive field weakening control or manufacturing defects. Such a failure can result in the machine to underperform in an application and endanger system functionality. This paper proposes a simple strategy to detect such uniform demagnetization through a time domain signal-based approach. Further, a demagnetization fault diagnosis system has the potential to generate a false positive under a position sensor fault. Therefore, the approach proposed in this paper includes a disambiguation strategy to separate position sensor offset faults from uniform demagnetization detection to prevent false positive. The proposed algorithm has been verified with simulation, and experimental results at multiple operating points and transient states validating the approach.

## REFERENCES

[1] J. Faiz and E. Mazaheri-Tehrani, "Demagnetization Modeling and Fault Diagnosing Techniques in Permanent Magnet Machines Under Stationary and Nonstationary Conditions: An Overview," in IEEE Transactions on Industry Applications, vol. 53, no. 3, pp. 2772-2785, May-June 2017, doi: 10.1109/TIA.2016.2608950.

[2] Z. Mynar, L. Vesely and P. Vaclavek, "PMSM Model Predictive Control with Field-Weakening Implementation," in *IEEE Transactions on Industrial Electronics*, vol. 63, no. 8, pp. 5156-5166, Aug. 2016, doi: 10.1109/TIE.2016.2558165.

[3] S. Chi, Z. Zhang and L. Xu, "Sliding-Mode Sensorless Control of Direct-Drive PM Synchronous Motors for Washing Machine Applications," in *IEEE Transactions on Industry Applications*, vol. 45, no. 2, pp. 582-590, March-april 2009, doi: 10.1109/TIA.2009.2013545.

[4] T. Sebastian, "Temperature effects on torque production and efficiency of PM motors using NdFeB magnets," in IEEE Transactions on Industry Applications, vol. 31, no. 2, pp. 353-357, March-April 1995, doi: 10.1109/28.370284.

[5] A. Sarikhani and O. Mohammed, "Real-time demagnetization assessment of PM synchronous machine," 2012 XXth International Conference on Electrical Machines, 2012, pp. 2418-2424, doi: 10.1109/ICElMach.2012.6350222.

[6] J. Zhao, L. Wang, L. Xu, F. Dong, J. Song and Y. Xing, "Uniform Demagnetization Diagnosis for Permanent Magnet Synchronous Linear Motor Using a Sliding-Mode Velocity Controller and an ALN-MRAS Flux Observer," in *IEEE Transactions on Industrial Electronics*, doi: 10.1109/TIE.2021.3050360.

[7] Y. Gritli, A. Tani, C. Rossi and D. Casadei, "Detection of Rotor Magnet Demagnetization in Asymmetrical Six-Phase Surface Mounted Permanent Magnet Synchronous Motor Drive," 2018 XIII International Conference on Electrical Machines (ICEM), 2018, pp. 1809-1814, doi: 10.1109/ICELMACH.2018.8506688.

[8] K. Ahsanullah, E. Jeyasankar, S. K. Panda, R. Shanmukha and S. Nadarajan, "Detection and analysis of winding and demagnetization faults in PMSM based marine propulsion motors," 2017 IEEE International Electric Machines and Drives Conference (IEMDC), 2017, pp. 1-7, doi: 10.1109/IEMDC.2017.8002050.

[9] J. Hong et al., "Detection and Classification of Rotor Demagnetization and Eccentricity Faults for PM Synchronous Motors," in IEEE Transactions on Industry Applications, vol. 48, no. 3, pp. 923-932, May-June 2012, doi: 10.1109/TIA.2012.2191253.

[10] J. Riba Ruiz, J. A. Rosero, A. Garcia Espinosa and L. Romeral, "Detection of Demagnetization Faults in Permanent-Magnet Synchronous Motors Under Nonstationary Conditions," in IEEE Transactions on Magnetics, vol. 45, no. 7, pp. 2961-2969, July 2009, doi: 10.1109/TMAG.2009.2015942.

[11] S. Rajagopalan, J. M. Aller, J. A. Restrepo, T. G. Habetler and R. G. Harley, "Detection of Rotor Faults in Brushless DC Motors Operating Under Nonstationary Conditions," in IEEE Transactions on Industry Applications, vol. 42, no. 6, pp. 1464-1477, Nov.-dec. 2006, doi: 10.1109/TIA.2006.882613.

[12] M. Zafarani, T. Goktas and B. Akin, "A Comprehensive Magnet Defect Fault Analysis of Permanent-Magnet Synchronous Motors," in IEEE Transactions on Industry Applications, vol. 52, no. 2, pp. 1331-1339, March-April 2016, doi: 10.1109/TIA.2015.2487440.

[13] J. Faiz and H. Nejadi-Koti, "Demagnetization Fault Indexes in Permanent Magnet Synchronous Motors—An Overview," in IEEE Transactions on Magnetics, vol. 52, no. 4, pp. 1-11, April 2016, Art no. 8201511, doi: 10.1109/TMAG.2015.2480379.

[14] T. Goktas, M. Zafarani, K. W. Lee, B. Akin and T. Sculley, "Comprehensive Analysis of Magnet Defect Fault Monitoring Through Leakage Flux," in IEEE Transactions on Magnetics, vol. 53, no. 4, pp. 1-10, April 2017, Art no. 8201010, doi: 10.1109/TMAG.2016.2617318.

[15] M. Zhu, W. Hu and N. C. Kar, "Acoustic Noise-Based Uniform Permanent-Magnet Demagnetization Detection in SPMSM for High-Performance PMSM Drive," in IEEE Transactions on Transportation Electrification, vol. 4, no. 1, pp. 303-313, March 2018, doi: 10.1109/TTE.2017.2755549.

[16] M. Zhu, W. Hu and N. C. Kar, "Multi-Sensor Fusion-Based Permanent Magnet Demagnetization Detection in Permanent Magnet Synchronous Machines," in IEEE Transactions on Magnetics, vol. 54, no. 11, pp. 1-6, Nov. 2018, Art no. 8110106, doi: 10.1109/TMAG.2018.2836182.

[17] S.S. Kuruppu," Position Sensor Harmonics Influence on Highly Integrated Field Oriented Controlled PMSM Drive Torque Output," *2021 IEEE Transportation Electrification Conference*, 2021,

[18] S. S. Kuruppu and Y. Zou, "Static Position Sensor Bias Fault Diagnosis in Permanent Magnet Synchronous Machines via Current Estimation," in *IEEE/ASME Transactions on Mechatronics*, vol. 26, no. 2, pp. 888-896, April 2021, doi: 10.1109/TMECH.2020.3010898.

[19] S. S. Kuruppu and Y. Zou, "Postproduction PMSM Position Sensor Offset Error Quantification via Voltage Estimation," *2020 IEEE Energy Conversion Congress and Exposition (ECCE)*, 2020, pp. 3355-3361, doi: 10.1109/ECCE44975.2020.9235757.

**Sunil A. Abeyratne** (Senior Member, IEEE) was born in Kandy, Sri Lanka. He received the B.Sc. Eng. degree in electrical and electronics engineering from the University of Peradeniya, Peradeniya, Sri Lanka, in 1987, and the M.Eng. and Ph.D. degrees from Gifu University, Gifu, Japan, in 1992 and 1997, respectively.

From 1987 to 1988, he was an Instructor with the Department of Electrical and Electronic Engineering, University of Peradeniya. In 1998, he joined the Colombo Dockyard Limited in the category of an Electrical and Electronic Engineer and worked until January 2000. He was a Researcher with the Wisconsin Power Electronics Research Center, University of Wisconsin Madison, Madison, WI, USA, from 1992 to 1994. From 1997 to 1998, he was a Software Engineer with Total Office O, Japan. He joined the University of Peradeniya as a Senior Lecturer in 1999. He has been with the Toshiba Schneider Inverter Corporation, Design and Development Group, Mie, Japan, as a Researcher/Trainee in 2001. Since 2017, he has been a Professor with the Faculty of Engineering, University of Peradeniya, Peradeniya, Sri Lanka.

**Sandun S. Kuruppu** (M'14–SM'19) received his B.S. degree in Electrical and Electronics Engineering from University of Peradeniya, Sri Lanka in 2007 and M.S. and Ph.D. degrees from Purdue University, West Lafayette, Indiana, USA, in 2010 and 2013, respectively.

He is an Associate Professor of Electrical and Computer Engineering at Saginaw Valley State University, Michigan, USA. Prior to his current position, he was with Nexteer Automotive, Texas Instruments Kilby Labs and Delphi Electronics and Safety. His current research interests include fault prognostics, diagnostics, localization, mitigation in mechatronic systems, power electronics, vehicle stability control, and extremum seeking controls for traction applications.